

Impact of Hydrogen in Ga-Doped Silicon on Maximum LeTID Defect Density

Ruben Zerfaß,* Jochen Simon, Axel Herguth, and Giso Hahn

Many studies suggest that hydrogen is an important factor for light and elevated temperature-induced degradation (LeTID) in p-type c-Si solar cells. The exact mechanism of this defect is still unknown. Here, Ga-doped Si wafers fired with an $\text{SiN}_x\text{:H}$ layer present were used to establish a correlation between the initial concentration of GaH pairs and H_2 dimers on one and the maximum defect density evolving during degradation on the other hand. Degradation of all samples is performed at constant excess charge carrier injection. The correlation to LeTID defect density is found to be linear in the case of $[\text{H}_2]$, hence, a direct involvement of H_2 in the defect formation is expected. In contrast, the correlation between GaH pairs and defects is found to scale with the fraction of GaH on total hydrogen concentration. This fraction is not constant but rather decreases with an increase in total hydrogen concentration. In addition, changes in $[\text{GaH}]$ and lifetime are examined under different degradation conditions with either fixed injection up to 10^{16}cm^{-3} and temperatures up to 180°C . Under these conditions, LeTID evolves but no dissociation of $[\text{GaH}]$ takes place. The effective activation energy of LeTID defect formation is determined to be $0.76(17)\text{ eV}$.

example, by varying the hydrogen release during a rapid thermal anneal (RTA) by changing the peak temperature^[2,9–12] or the properties of the hydrogen-rich $\text{SiN}_x\text{:H}$ layer.^[5,6,13] In another study, Bredemeier et al. investigated the diffusion of the defect precursor and found a correspondence with the diffusion of H in c-Si.^[14] In addition, a quantitative correlation between hydrogen concentration and defect density was found in B-doped multi-Si^[15] as well as in B-doped Czochralski grown Si^[16] and float zone Si.^[17] These quantitative correlations are important because they can provide information on the defect composition and thus enable the understanding of LeTID.

In all these contributions, degradation occurred under isogenerative conditions, meaning that the excess charge carrier concentration (injection) was not constant during degradation as it depends on the defect concentration that changes with time.

Unfortunately, defect dynamics and also the observed maximum defect density depend on the injection,^[18,19] hence complicating the analysis with respect to other influencing factors like the hydrogen concentration. Furthermore, it is important to clarify whether the trends found in B-doped material also apply to Ga-doped material, i.e., whether the defect exhibits the same characteristics independent of the dopant.


In this contribution, the correlation between hydrogen concentration in the Si bulk and LeTID defect density is investigated in Ga-doped Cz-Si. Here, the samples are degraded at constant injection^[20] to explicitly exclude the dependency of maximum defect density on injection. The concentration of hydrogen in the Si bulk is determined by means of highly sensitive resistivity measurements.^[21,22] This technique is advantageous compared to the detection of hydrogen species by Fourier transform infrared spectroscopy (FTIR) (e.g., Refs. [17,23]) because it requires much less experimental effort and allows repeated measurements during degradation. At the same time, resistivity measurement has a better detection limit than secondary ion mass spectroscopy (SIMS).^[24] As a result, an improved correlation can be obtained, which allows for accurate conclusions on the influence of the hydrogen species H_2 and GaH pairs on defect formation. In addition, the influence of degradation conditions, i.e., injection and temperature, is investigated.

1. Introduction

The light- and elevated temperature-induced degradation (LeTID) of crystalline silicon solar cells is an efficiency limiting effect affecting B- and Ga-doped materials.^[1] Although there have been studies on ways to suppress it as far as possible by suitable processing,^[2–8] the true nature of this defect is still unclear.

Hydrogen, originating from dielectric passivation layers such as $\text{SiN}_x\text{:H}$, is shown to play a critical role in this defect. This has been demonstrated in several ways: There are numerous studies that determine the H content of the wafers indirectly, for

R. Zerfaß, J. Simon, A. Herguth, G. Hahn
Department of Physics
University of Konstanz
Universitätsstraße 10, 78457 Konstanz, Germany
E-mail: ruben.zerfass@uni-konstanz.de

 The ORCID identification number(s) for the author(s) of this article can be found under <https://doi.org/10.1002/solr.202300501>.

© 2023 The Authors. Solar RRL published by Wiley-VCH GmbH. This is an open access article under the terms of the Creative Commons Attribution-NonCommercial-NoDerivs License, which permits use and distribution in any medium, provided the original work is properly cited, the use is non-commercial and no modifications or adaptations are made.

DOI: 10.1002/solr.202300501

2. Results and Discussion

2.1. Influence of Sample Preparation

2.1.1. Linear Correlation of H_2 and Defects

Hydrogen is introduced into the Si bulk by diffusion from the $SiN_x:H$ passivation layer during the fast firing step applied during solar cell manufacturing. The amount of hydrogen that is diffused into the Si bulk by this step depends among other things on the peak firing temperature.^[25,26] This was used in this experiment to achieve a wide variation in hydrogen concentration by varying the peak temperature of the belt furnace, for which values between 709 and 816 °C were measured.

In p-type Si, hydrogen is present after RTA mainly either as H_2 dimer or as an overall neutral acceptor-hydrogen pair,^[27,28] in particular as Ga^-H^+ in our case. Additional GaH pairs can be formed from H_2 dimers if samples are annealed in the dark according to the overall reaction scheme



whereby the applied 4 h at 180 °C should suffice to dissociate almost all dimers.^[29] Since the splitting of H_2 requires two holes h^+ , it is possible to calculate the concentration $[H_2]$ from half the difference in initial hole concentration p_{init} and hole concentration after dark anneal p_{da}

$$[H_2]_{init} = \frac{1}{2}(p_{init} - p_{da}) \quad (2)$$

In a next step, the samples undergo an illuminated anneal at approximately two suns equivalent^[30] and a temperature of 300 °C. This process leads to the dissociation of the GaH pairs into an unknown species^[31] whereby holes are released again. After ≈ 11 h, the hole concentration of the samples saturates, which is interpreted as the dissociation of all or most of the GaH pairs.^[31] Thus, the initial concentration of GaH is given by the difference of the hole concentration in the initial state p_{init} and after the illuminated anneal p_{ia} .

$$[GaH]_{init} = p_{ia} - p_{init} \quad (3)$$

For the calculation of the two quantities (2) and (3), the assumption was made that hole concentration changes only due to pair formation. In this temperature range, no other processes are reported that are able to change hole concentration in the order of 10^{14} cm^{-3} , except for thermal donors. These form significantly later compared to the GaH pair dynamics,^[32] so that the influence is negligible. Also, it was assumed that the majority of H_2 participates in the pair formation mechanism.

The method described above allows for a reliable detection of the initial H_2 and GaH concentration. In order to investigate how these concentrations affect the formation of LeTID defects, two $5 \times 5 \text{ cm}^2$ sister samples were cut from each wafer after the firing step. This ensures both samples to have experienced the same firing profile independent of fluctuations of the belt furnace in between wafers. One of these sample then is used for $[H_2]_{init}$ and $[GaH]_{init}$ determination while the other sample is degraded at a constant excess charge carrier injection of $\Delta n =$

10^{15} cm^{-3} until the maximum defect concentration was reached. The change in lifetime-equivalent defect density ΔN_{leq} ^[33] was calculated from the change in excess charge carrier lifetime τ measured during degradation and evaluated at $\Delta n = 1.5 \times 10^{15} \text{ cm}^{-3}$ with respect to the initial lifetime τ_0

$$\Delta N_{leq} = \frac{1}{\tau_0} - \frac{1}{\tau} \quad (4)$$

From this, the maximum defect density ΔN_{max} was extracted using the exponential rise-to-maximum function (as a solution to first-order reactions with constant rate)

$$\Delta N_{leq}(t) = \Delta N_{max}(1 - \exp(-R_{deg} \times t)) \quad (5)$$

where R_{deg} denotes for the specific rate of the degradation process.

These two evaluations allow to correlate the initial hydrogen species concentration ($[H_2]_{init}$, $[GaH]_{init}$) and the maximum defect density ΔN_{max} . The resulting data is presented in **Figure 1**. A wide range of both defect density and initial concentrations is shown as the firing temperature was varied from 709 to 816 °C as indicated by the color map.

At first glance, both hydrogen species, $[GaH]_{init}$ and $[H_2]_{init}$, appear to increase linearly with ΔN_{leq} following a similar slope. While it can be argued that the intersection of the $[H_2]_{init}$ linear trend line with the origin is smeared out due to uncertainties during the measurements, this is not the case for $[GaH]_{init}$. Here, a linear trend line would be clearly shifted by about $3 \times 10^{14} \text{ cm}^{-3}$ towards higher concentrations. A linear correlation in the case of $[GaH]_{init}$ would mean that a certain amount of $3 \times 10^{14} \text{ cm}^{-3}$ of initial GaH pairs could be present in the Si without LeTID occurring.

It is unlikely that GaH pairs act as defect precursor above a certain threshold only but not at all for fewer pairs. Hence, GaH pairs are presumably not involved in defect formation at all, and more likely the observed correlation is not of causal

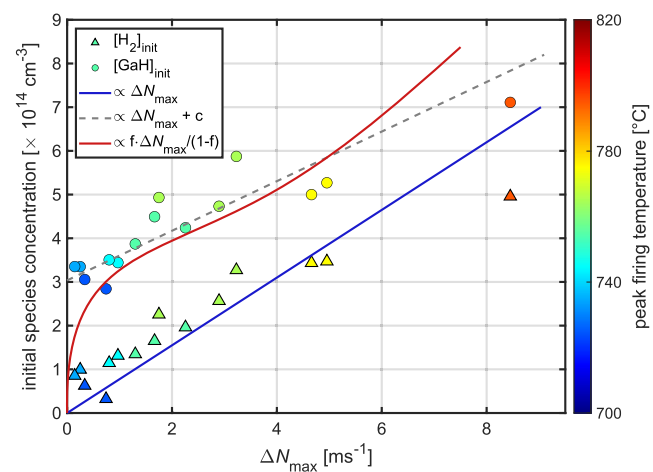


Figure 1. Dependence of the maximum defect concentration, quantified by the maximum of lifetime equivalent defect density ΔN_{max} on the concentration of the initial hydrogen species H_2 and GaH. The correlation with H_2 is fitted by a linear approach, whereas the curved correlation with GaH is derived in Section 2.1.2.

nature but rather a side effect. In contrast, the fairly good linear relationship between $[H_2]_{\text{init}}$ and ΔN_{max} points toward the H_2 dimer as the relevant source of hydrogen for LeTID. However, the initial concentrations of GaH and H_2 are not independent from each other. Both are linked to the temperatures encountered during RTA, in particular the cool-down phase, when both H_2 and GaH form from atomic hydrogen or exchange hydrogen with each other as they do during dark and illuminated annealing. Insofar, it seems logical that there is some relationship between $[H_2]_{\text{init}}$ and $[GaH]_{\text{init}}$ and this might explain why ΔN_{max} scales with $[GaH]_{\text{init}}$, even though GaH pairs might not trigger LeTID. In other words, it is not possible to prepare a sample with independent concentrations of H_2 and GaH, in particular it is not possible to prepare a sample containing only GaH pairs, but no H_2 dimers at all. As soon as there are GaH pairs, there are also H_2 dimers and thus a nonvanishing defect density.

That is why there is not a linear relationship of ΔN_{max} and $[GaH]$. There is no intersection with the y-axis, but rather a curvature toward the origin. The justification of the drawn course will be given in the next section.

2.1.2. Fraction of GaH Pairs on Total H Concentration

As the experimental data suggest, there seems to be a true linear dependence of maximum LeTID defect concentration on initial hydrogen dimer concentration, i.e., $\Delta N_{\text{max}} \propto [H_2]_{\text{init}}$. If this is the case, the dependency of defect concentration on total hydrogen concentration $[H]$ or pair concentration $[GaH]$ should not be directly proportional as discussed in the following. Total hydrogen concentration corresponds to hydrogen bound in dimers and pairs, i.e., $[H] = 2[H_2] + [GaH]$. Then defect density scales as $\Delta N_{\text{max}} \propto \frac{1}{2}([H] - [GaH])$. If the pair concentration is expressed as a fraction f of total hydrogen, so that $[GaH] = f[H]$, the above equation simplifies to either $\Delta N_{\text{max}} \propto \frac{1}{2}[H](1 - f)$ or $\Delta N_{\text{max}} \propto \frac{1}{2}[GaH](f^{-1} - 1)$. If this fraction would be constant, defect density would be proportional to both, $[H]$ and $[GaH]$. However, the experiment suggests that this fraction f is not constant, but depends on the hydrogen concentration itself as can be seen in **Figure 2**. In consequence, defect density does not scale linearly with pair concentration, or at least not over the whole range of hydrogen concentrations. In the experiment, f seems to decay more or less exponentially with $[H]$, potentially saturating around a value of 0.4. In this saturation region, ΔN_{max} should scale linearly with both $[H]$ and $[GaH]$, but with a certain offset shifting the line to higher $[H]$ or $[GaH]$. As discussed earlier, extrapolating this linear trend valid at high $[H]$ to zero ΔN_{max} then produces an axis intercept that could be interpreted as a critical concentration of $[H]$ or $[GaH]$ below that no defect formation occurs, simply because no $[H_2]$ exists. However, this is a misinterpretation because the dependence of ΔN_{max} becomes nonlinear toward low concentrations. The experimental data suggest that f increases toward low $[H]$ concentrations, implying that the GaH concentration should bend toward the origin. The exact progression cannot be concluded from the experimental data not covering concentrations below $3 \times 10^{14} \text{ cm}^{-3}$ but for reasons of consistency it is clear that $f = [GaH]/[H]$ cannot exceed unity. It seems reasonable to assume that f approaches, but does not become unity toward zero $[H]$ concentrations, so that the empirical trend curve in **Figure 2** should start

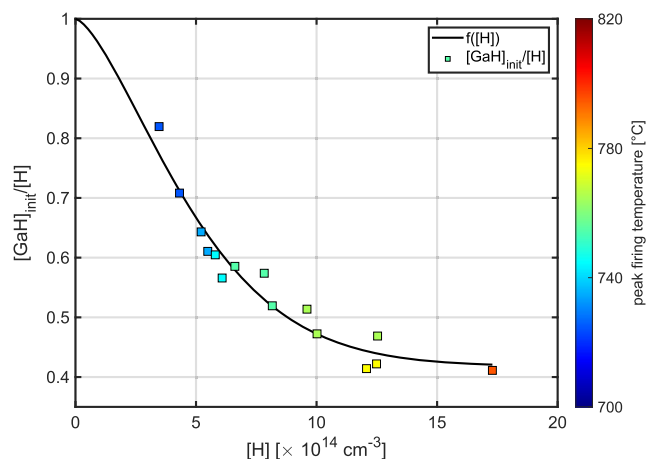


Figure 2. Share of the hydrogen initially bound as GaH-pairs dependent on the total concentration of hydrogen in the sample. Different hydrogen concentrations are achieved by varying the peak temperature during the firing step.

at (0|1). Therefore, the trend curve of $[GaH]$ vs ΔN_{max} in **Figure 1** should start at the origin. In fact, the curved line in **Figure 1** calculated with the described approach and f from **Figure 2** matches the experimental data quite well even though the bending toward origin is not covered by the data. It is very likely that the fraction f of GaH pairs in the total hydrogen concentration also depends on the temperature profile, in particular the cooling rate, during the firing process. Therefore, a different f may be expected for other firing processes. The firing profiles of the samples shown here are given in the Supporting Information for comparison.

In summary, hydrogen favors pairs over dimers, the stronger the lower $[H]$, but even at lowest concentrations a few dimers are expected to form that could trigger defect formation. Overall, this is good news for the mitigation of LeTID because it means that the lower the hydrogen concentration gets, the less defects can be formed from H_2 because hydrogen prefers to form stable GaH pairs instead of H_2 during firing/cool down.

2.2. Influence of Degradation Conditions

2.2.1. Injection Dependence

Figure 3 shows the lifetime equivalent defect density ΔN_{leq} and the change in hole concentration Δp over the course of a degradation treatment. During this process, injection in the sample is fixed by varying the illumination intensity accordingly. These measurements were conducted for a range of different injection levels between 7.5×10^{14} and $1 \times 10^{16} \text{ cm}^{-3}$. Furthermore, one sample was treated without any illumination.

The degradation and regeneration of ΔN_{leq} are fitted with the sum of two exponential functions as shown in Equation (6), of which one represents the degradation with the rate R_{deg} , while the other one describes the slower running regeneration process with the rate R_{reg} . The prefactors $N_{\text{reg/deg}}$ scale with the maximum amount of degradation and regeneration, respectively. The constant $c = N_{\text{reg}} - N_{\text{deg}}$ ensures that ΔN_{leq} start at 0 as given by its definition in Equation (4).

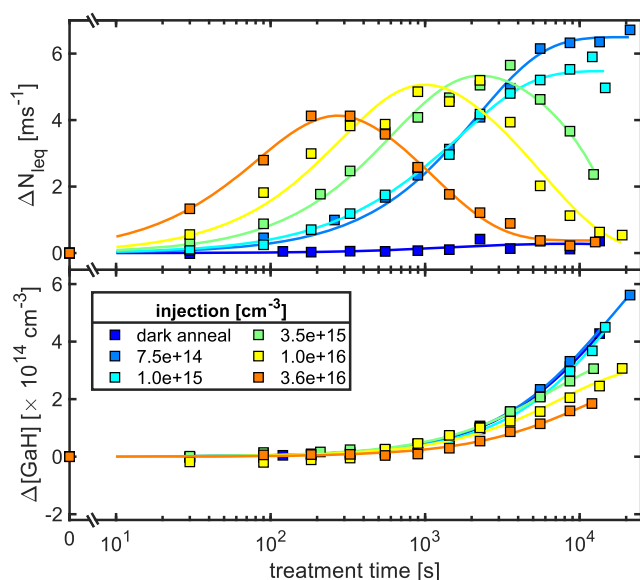


Figure 3. Change in lifetime equivalent defect density ΔN_{leq} and pair concentration $\Delta[\text{GaH}]$ during the course of a treatment at 120 °C and illumination with different, but in each case constant, charge carrier injection.

$$\Delta N_{\text{leq}}(t) = N_{\text{deg}} \times \exp(-R_{\text{deg}} \times t) - N_{\text{reg}} \times \exp(-R_{\text{reg}} \times t) + c \quad (6)$$

Between all those samples, clear differences in the behavior of the defect density are visible. The strongest difference is found when comparing the defect density of the sample degraded in the dark with the illuminated samples. The degradation effect in the nonilluminated sample is an order of magnitude smaller than in the illuminated ones, so it is difficult to see in the graph. This contrasts with studies on B-doped samples, which also show strong degradation in the dark.^[10] However, whether the effect is actually due to the dopant or merely to differences in sample preparation cannot be answered comprehensively due to a lack of data in literature. If injection is increased, the degradation phenomenon occurs faster. Also, this affects the regeneration phase such that regeneration is only visible for high carrier injections due to the limited treatment time of around 10 h. There is no indication of surface-related degradation during treatment as the saturation current density J_0 , evaluated by difference analysis,^[34] remains constant during treatment. The amplitude of the defect density ΔN_{max} seems to lower with an increase in injection. This effect might be caused by three possible reasons: 1) a reduced formation of defects with an increasing injection, 2) a changing ratio of R_{deg} and R_{reg} implying a change in observable amplitude of degradation, or 3) differences in the total hydrogen concentration due to fluctuations during sample processing, which would lead to a different amount of degradation. Hence, no reliable statement can be made about the dependence of the maximum defect density on the injection, as variations during processing cannot be excluded and the ratio of R_{deg} and R_{reg} cannot be evaluated due to the lack of data during regeneration. However, since there is a strong dependence of the time constant on injection, defect formation is an electron-driven process. Numerous previous studies also came to this conclusion.^[10,35–37]

The lower part in Figure 3 shows the change in GaH pair concentration obtained from the change in resistivity over the course of the degradation on the same sample. In the case of the dark anneal, the pair concentration increases continuously over the course of the experiment. This is attributed to the formation of GaH pairs from H_2 present in the Si after firing. Low injection levels up to $1 \times 10^{15} \text{ cm}^{-3}$ exhibit an almost identical behavior in the pair concentration. A further rise of the injection level up to $3.6 \times 10^{16} \text{ cm}^{-3}$ leads to a flattening of the increase in $[\text{GaH}]$. Still, additional pairs are formed, but the saturation value seems to be lower. In principle, the same limitations on the evaluation of the maximum pair concentration as in the case of the maximum defect concentration apply. However, the equilibrium between H_2 and formed pairs is known to be dependent on injection,^[31] shifting away from pairs toward dimers with increasing injection, and the data shown follow this trend.

In conclusion, no dissociation of GaH pairs can be observed during degradation immediately after the RTA. In this respect, GaH pairs do not contribute to the hydrogen budget from which LeTID is supplied. However, this characteristic only applies to the state immediately after the RTA, as investigated here. If additional pairs are formed prior to degradation by other processes, such as dark annealing, GaH could also dissociate under the conditions studied here until an equilibrium is reached. A mitigation strategy based on forming GaH pairs prior to degradation may therefore fail to prevent LeTID.

2.2.2. Temperature Dependence

Similar measurements to those presented before but now with different annealing temperatures and a fixed injection of 10^{15} cm^{-3} are shown in Figure 4. It is apparent that a higher

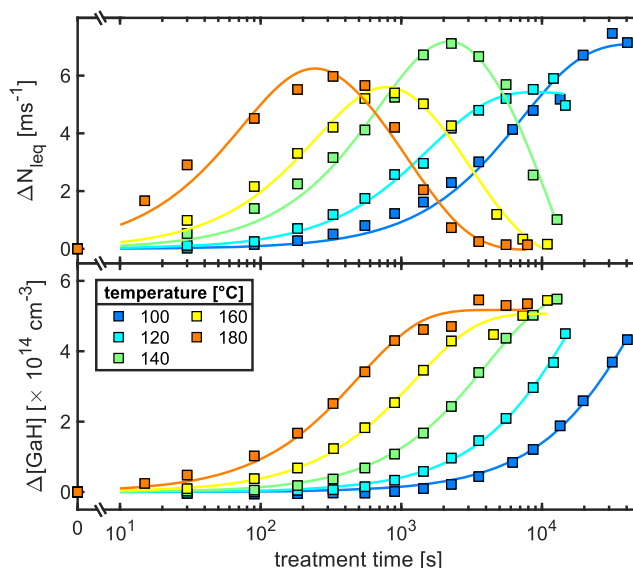


Figure 4. Change in lifetime equivalent defect density ΔN_{leq} and pair concentration $\Delta[\text{GaH}]$ during degradation at different temperatures. Illumination of the samples is adapted to allow a constant carrier injection of 10^{15} cm^{-3} .

temperature causes a faster degradation and regeneration of the sample. In contrast to the variation in carrier injection, the variation of temperature changes the timescale on which the formation of GaH pairs takes place.

From the data shown earlier, it is visible that there is no dissociation of GaH pairs under typical conditions as used for the degradations examined in Section 2.1. As a consequence of this, no additional H₂ is released during degradation. However, dissociation of GaH pairs may still occur at higher temperatures or injection.

Determination of the Activation Energy: To determine the activation energy of the defect, the time constants of the degradation R_{deg} resulting from the fits of Equation (6) are plotted in **Figure 5** against the inverse of the degradation temperature T .

The correlation between temperature and degradation rate is well described by Arrhenius' law

$$R_{\text{deg}}(T) = R_0 \cdot \exp\left(-\frac{E_A}{k_B T}\right) \quad (7)$$

where k_B is the Boltzmann's constant, R_0 is the temperature-independent prefactor, and E_A is the effective activation energy of the defect. A fit according to this equation is also shown in **Figure 5**.

From this, E_A is determined to be 0.76(17) eV. This value fits well with other activation energies determined in the literature. Jafari et al. found this value to be 0.74(10) eV, while Winter et al. determined 0.58(4) eV.^[38] Lin et al. noticed a two-step degradation process with the respective activation energies 0.96(4) and 0.90(5) eV.^[39] In the data presented here, there are no indications for such a two-step process. This may be a consequence of constant carrier injection during degradation rather than constant illumination used in the cited study above. It could also be that two-step degradation can only be observed at lower temperatures and/or injections. Furthermore, the effective activation energy is also dependent on the firing temperature^[20] and might depend on the injection during degradation.

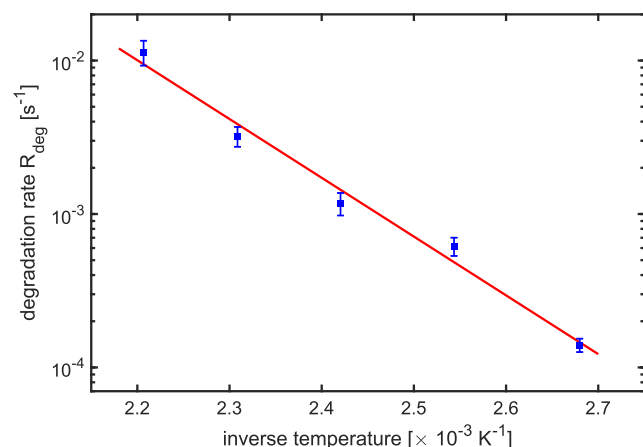


Figure 5. Degradation rate from exponential fit plotted over the inverse of the temperature during degradation. The red line is a fit according to Arrhenius' law from which the activation energy of the defect is determined as $E_A = 0.76(17)$ eV.

3. Conclusion

The relationship between the initial hydrogen dimer concentration $[\text{H}_2]$ and the defect density in Ga-doped Si appears to be linear over the range of concentrations studied. This result is in good agreement with a previous investigation in B-doped multi-crystalline Si.^[15]

This suggests that the LeTID defect in both materials is composed of hydrogen and that the available amount of H₂ determines the defect concentration. In addition, this finding is consistent with hypotheses about the microscopic structure of the defect that require H₂ as a precursor for LeTID.^[40–43] In contrast, degradation is not affected by the initially present GaH pairs. Right after RTA, hydrogen tends to favor GaH pairs over H₂ dimers the lower the overall hydrogen concentration. This is conducive to the mitigation of LeTID by hydrogen reductions, since disproportionately more initial GaH pairs with decreasing H concentration means disproportionately less initial H₂ dimers and thus less LeTID defects that can arise from them. Or in other words, it gets easier to mitigate LeTID the lower the hydrogen concentration gets. Furthermore, it has been shown that in our case GaH pairs do not dissociate under typical degradation conditions, but on the contrary resemble hydrogen sinks, at least when the initial GaH pair concentration is lower than its equilibrium value. The duration of LeTID formation strongly depends on temperature and excess charge carrier injection. The effective activation energy for the formation of the defect is 0.76(17) eV. A strong dependence of the maximum extent of degradation on injection or temperature cannot be observed in the data shown.

4. Experimental Section

Preprocessing: For all experiments, Ga-doped Cz-Si wafers with a resistivity of 1.0 $\Omega \text{ cm}$ were used. After saw damage etching (KOH at 80 °C for 8 min) and wet chemical cleaning (H₂O₂:O₃ and subsequent HF dip), a SiN_x:H passivation layer was deposited to both sides using plasma-enhanced chemical vapor deposition (PECVD). The SiN_x:H layers featured a thickness of 75 nm and a refractive index of 2.0 as this is a common antireflective coating.

Firing: All wafers were fired using an industrial belt furnace (centrotherm c.fire9000). The temperature profile during this process was measured multiple times before and after the actual firing step on a dummy wafer that experienced identical preprocessing steps. Temperature measurements were performed with a data logger and a k-type thermocouple which was pressed onto the center of the wafer. For the first part of the experiments, wafers were fired in small batches at different temperatures in the range between 700 and 820 °C in order to vary the amount of hydrogen introduced into the sample. For the experiments on injection and temperature dependence of the degradation, all wafers were fired as one group at the same temperature of 795 °C. In all cases, about 15 dummy wafers with the same optical properties were sent ahead of the actual process wafers at intervals of 5 s to stabilize the belt furnace. From every wafer, two $5 \times 5 \text{ cm}^2$ sized samples were cut from the front half with an IR laser.

Iso-Injunctive Degradation: During iso-injunctive degradation, the samples were illuminated using a laser at 805 nm wavelength with adjustable power that was widened to cover the full area of the sample using a beam homogenizer. During the degradation, excess charge carrier lifetime τ was measured using a temperature-controlled PCD setup (WCT-120TS, Sinton Instruments) set to the degradation temperature. The photon flux of the laser was adjusted such that the charge carrier generation rate G fulfills the condition of a constant excess charge carrier concentration Δn in the sample

$$G = \frac{\Delta n}{\tau} \quad (8)$$

Further details of this procedure are published elsewhere.^[20]

Hole Concentration Measurement: Since the hydrogen concentration was derived from the change in hole concentration, direct resistivity measurements were performed on the samples. Therefore, two pairs of stripe-like Al-pads were evaporated on opposing sides of the samples using an electron-beam vapor deposition. Electrical contact to the substrate through the passivation layer was achieved by laser-fired contacts (LFC).^[44] Resistivity measurements were performed on a temperature-stabilized 4-terminal setup,^[22] and the hole concentration was calculated with hole mobility data obtained from PVlighthouse.^[45] For the detection of initial hydrogen in Section 2.1, the formation of GaH pairs was triggered by a dark anneal at 180 °C for 4 h on a hotplate (*praezitherm*). To dissociate these pairs again, samples were annealed at 300 °C for 11 h at the photon flux equivalent to 2 suns with halogen lamps.^[30] For Section 2.2, the hole concentration p_i was monitored frequently during the degradation. From the change in hole concentration during treatment of the sample, the change in pair concentration $\Delta[\text{GaH}] = p_{\text{init}} - p_i$ with respect to the initial value was calculated.

Acknowledgements

The authors would like to thank Joshua Kamphues for support in J_0 analysis. Part of this work was funded by German Federal Ministry for Economic Affairs and Climate Action (BMWK) under contract number 03EE0152A. The content is the responsibility of the authors.

Open Access funding enabled and organized by Projekt DEAL.

Conflict of Interest

The authors declare no conflict of interest.

Data Availability Statement

The data that support the findings of this study are available from the corresponding author upon reasonable request.

Keywords

Ga-doped Si, GaH pairs, hydrogen, LeTID

Received: June 30, 2023

Revised: September 1, 2023

Published online: September 22, 2023

- [1] K. Ramspeck, S. Zimmermann, H. Nagel, A. Metz, Y. Gassenbauer, B. Birkmann, A. Seidl, in *Proc. 27th Eur. Photovoltaic Solar Energy Conf.*, WIP, Munich **2012**, pp. 861–865.
- [2] R. Eberle, W. Kwapil, F. Schindler, M. C. Schubert, S. W. Glunz, *Phys. Status Solidi RRL* **2016**, *10*, 861.
- [3] R. Sharma, A. G. Aberle, J. B. Li, *Sol. RRL* **2018**, *2*, 1800070.
- [4] C. Sen, M. Kim, D. Chen, U. Varshney, S. Liu, A. Samadi, A. Ciesla, S. R. Wenham, C. E. Chan, C. Chong, M. D. Abbott, B. J. Hallam, *IEEE J. Photovolt.* **2019**, *9*, 40.
- [5] U. Varshney, M. Abbott, A. Ciesla, D. Chen, S. Liu, C. Sen, M. Kim, S. Wenham, B. Hoex, C. Chan, *IEEE J. Photovolt.* **2019**, *9*, 601.
- [6] U. Varshney, M. Kim, M. U. Khan, P. Hamer, C. Chan, M. Abbott, B. Hoex, *IEEE J. Photovolt.* **2021**, *11*, 65.
- [7] C. Sen, C. Chan, P. Hamer, M. Wright, C. Chong, B. Hallam, M. Abbott, *Sol. Energy Mater. Sol. Cells* **2020**, *209*, 110470.
- [8] F. Maischner, S. Maus, J. Greulich, S. Lohmüller, E. Lohmüller, P. Saint-Cast, D. Ourinson, H. Vahlman, K. Hergert, S. Riepe, S. Glunz, S. Rein, *Prog. Photovolt.* **2021**, *30*, 123.
- [9] a) F. Kersten, P. Engelhart, H.-C. Ploigt, A. Stekolnikov, T. Lindner, F. Stenzel, M. Bartzsch, A. Szpeth, K. Petter, J. Heitmann, J. W. Müller, *Sol. Energy Mater. Sol. Cells* **2015**, *142*, 83; b) Proc. of the 5th Int. Conf. on Crystalline Silicon Photovoltaics (SiliconPV 2015).
- [10] D. Chen, M. Kim, B. V. Stefani, B. J. Hallam, M. D. Abbott, C. E. Chan, R. Chen, D. N. Payne, N. Nampalli, A. Ciesla, T. H. Fung, K. Kim, S. R. Wenham, *Sol. Energy Mater. Sol. Cells* **2017**, *172*, 293.
- [11] T. Niewelt, F. Schindler, W. Kwapil, R. Eberle, J. Schön, M. C. Schubert, *Prog. Photovolt.* **2018**, *26*, 533.
- [12] C. Vargas, K. Kim, G. Coletti, D. Payne, C. Chan, S. Wenham, Z. Hameiri, *IEEE J. Photovolt.* **2018**, *8*, 413.
- [13] D. Bredemeier, D. C. Walter, R. Heller, J. Schmidt, *Phys. Status Solidi RRL* **2019**, *13*, 1900201.
- [14] D. Bredemeier, D. C. Walter, J. Schmidt, *Sol. RRL* **2018**, *2*, 1700159.
- [15] J. Schmidt, D. Bredemeier, D. C. Walter, *IEEE J. Photovolt.* **2019**, *9*, 1497.
- [16] S. Jafari, U. Varshney, B. Hoex, S. Meyer, D. Lausch, *IEEE J. Photovolt.* **2021**, *11*, 1363.
- [17] B. Hammann, N. Assmann, P. M. Weiser, W. Kwapil, T. Niewelt, F. Schindler, R. Sondenå, E. V. Monakhov, M. C. Schubert, *IEEE J. Photovolt.* **2023**, *13*, 224.
- [18] D. Chen, P. Hamer, M. Kim, C. Chan, A. C. nee Wenham, F. Rougieux, Y. Zhang, M. Abbott, B. Hallam, *Sol. Energy Mater. Sol. Cells* **2020**, *207*, 110353.
- [19] W. Kwapil, J. Dalke, R. Post, T. Niewelt, *Sol. RRL* **2021**, *5*, 2100147.
- [20] A. Graf, A. Herguth, G. Hahn, *AIP Conf. Proc.* **2019**, *2147*, 140003.
- [21] D. C. Walter, D. Bredemeier, R. Falster, V. V. Voronkov, J. Schmidt, *Sol. Energy Mater. Sol. Cells* **2019**, *200*, 109970.
- [22] A. Herguth, C. Winter, *IEEE J. Photovolt.* **2021**, *11*, 1059.
- [23] P. M. Weiser, E. Monakhov, H. Haug, M. S. Wiig, R. Sondenå, *J. Appl. Phys.* **2020**, *127*, 065703.
- [24] S. Schwarz, in *Encyclopedia of Materials: Science and Technology* (Eds: K. J. Buschow, R. W. Cahn, M. C. Flemings, B. Ilshner, E. J. Kramer, S. Mahajan, P. Veyssière), Elsevier, Oxford **2001**, pp. 8283–8290.
- [25] J. Hong, W. M. M. Kessels, W. J. Soppe, A. W. Weeber, W. M. Arnoldbik, M. C. M. van de Sanden, *J. Vac. Sci. Technol., B: Microelectron.* **2003**, *21*, 2123.
- [26] S. Wilking, S. Ebert, A. Herguth, G. Hahn, *J. Appl. Phys.* **2013**, *114*, 194512.
- [27] B. Hourahine, R. Jones, S. Öberg, R. C. Newman, P. R. Briddon, E. Roduner, *Phys. Rev. B* **1998**, *57*, R12666.
- [28] R. E. Pritchard, J. H. Tucker, R. C. Newman, E. C. Lightowers, *Semicond. Sci. Technol.* **1999**, *14*, 77.
- [29] Y. Acker, J. Simon, A. Herguth, *Phys. Status Solidi A* **2022**, *219*, 2200142.
- [30] A. Herguth, *Energy Procedia* **2017**, *124*, 53.
- [31] J. Simon, A. Herguth, L. Kutschera, G. Hahn, *Phys. Status Solidi RRL* **2022**, *16*, 2200297.
- [32] C. Winter, J. Simon, A. Herguth, *Phys. Status Solidi A* **2021**, *218*, 2100220.
- [33] A. Herguth, *IEEE J. Photovolt.* **2019**, *9*, 1182.
- [34] A. Herguth, J. Kamphues, *IEEE J. Photovolt.* **2023**, *13*, 672.
- [35] D. N. R. Payne, C. E. Chan, B. J. Hallam, B. Hoex, M. D. Abbott, S. R. Wenham, D. M. Bagnall, *Phys. Status Solidi RRL* **2016**, *10*, 237.
- [36] C. Vargas, G. Coletti, C. Chan, D. Payne, Z. Hameiri, *Sol. Energy Mater. Sol. Cells* **2019**, *189*, 166.
- [37] Z. Hu, L. Song, D. Lin, T. Zhao, Q. He, S. Yuan, X. Yu, D. Yang, *Sol. Energy* **2022**, *235*, 12.
- [38] M. Winter, D. C. Walter, J. Schmidt, *IEEE J. Photovolt.* **2021**, *11*, 866.

- [39] D. Lin, Z. Hu, L. Song, D. Yang, X. Yu, *Sol. Energy* **2021**, 225, 407.
- [40] J. A. T. De Guzman, V. P. Markevich, J. Coutinho, N. V. Abrosimov, M. P. Halsall, A. R. Peaker, *Sol. RRL* **2022**, 6, 2100459.
- [41] A. R. Meyer, P. C. Taylor, V. LaSalvia, X. Wang, W. Nemeth, M. Page, D. L. Young, S. Agarwal, P. Stradins, *Cell Rep. Phys. Sci.* **2023**, 4, 101201.
- [42] C. Chirag Mule, P. C. Taylor, A. Meyer, S. Agarwal, W. Nemeth, V. LaSalvia, M. Page, P. Stradins, in *Proc. of the 13th SiliconPV 2023*. **2023** (unpublished).
- [43] T. O. Abdul Fattah, V. P. Markevich, D. Gomes, J. Coutinho, N. V. Abrosimov, I. D. Hawkins, M. P. Halsall, A. R. Peaker, *Sol. Energy Mater. Sol. Cells* **2023**, 259, 112447.
- [44] E. Schneiderlöchner, R. Preu, R. Lüdemann, S. W. Glunz, *Prog. Photovoltaics* **2002**, 10, 29.
- [45] PV Lighthouse, Mobility Calculator, <https://www2.pvlighthouse.com.au/calculators/mobility%20calculator/mobility%20calculator.aspx> (accessed: June 2023).